MDPI

Article

A Dimension-Reduced Line-Element Method to Model Unsaturated Seepage Flow in Porous Media

Min Li [1], Xiaobo Zhang [2,*], Guoliang Su [1], Chenglong Fan [2], Qiang Zhang [1], Le Yi [2] and Tianyu Jing [1]

[1] GD Power Inner Mongolia New Energy Development Co., Ltd., Hohhot 010010, China; 12077682@ceic.com (M.L.); 12003353@ceic.com (G.S.); 12074377@ceic.com (Q.Z.); 12070930@ceic.com (T.J.)
[2] School of Infrastructure Engineering, Nanchang University, Nanchang 330031, China; fclgjy@163.com (C.F.); 412500220055@email.ncu.edu.cn (L.Y.)
*   Correspondence: zhangxb@ncu.edu.cn

Abstract: Contrary to the continuum hypothesis, which averages water flow across the entire domain, including both grains and pores, the line-element model concentrates unsaturated flow in the pore space in the intermediate region of horizontal and vertical channels. The flux equivalent principle is used to deduce the equivalent unsaturated hydraulic conductivity, the flow velocity and the continuity equations. It is found that the relative hydraulic conductivities derived from the line-element model and the continuum model are identical. The continuity equations in the two models are also similar, except that the coefficient in the water content term is half that in the line-element model. Thus, the unsaturated flow problem in porous media is transformed into a one-dimensional problem. A dimension-reduced finite line-element method is proposed that includes a complementary algorithm for Signorini's-type boundary conditions involving the seepage-face boundary and the infiltration boundary. The validity of the proposed model is then proved by good agreement with analytical, experimental and simulated results for one-dimensional infiltration in a vertical soil column, unsaturated flow in a sand flume with drainage tunnels, and transient unsaturated flow water-table recharge in a soil slab, respectively. In general, the proposed method has good computational efficiency, especially for smaller mesh sizes and short time intervals.

Keywords: unsaturated flow; line element; porous media; water pressure head; water table

1. Introduction

Numerical analysis of unsaturated flow behavior in porous media is fundamental in geotechnical engineering problems involving precipitation-induced landslides [1–3], dam failure of a tailing [4,5], seepage control in concrete construction [6–8] and CO_2 sequestration [9].

Because of the heterogeneity of grain and pore sizes, the nonlinearity of hydraulic constitutive relationships and the variability of boundary conditions, substantial efforts have been made to solve the Richards' equation [10] by numerical approaches, such as the finite element method [11,12], the finite difference method [13], the finite volume method [14] and the numerical manifold method [15]. To solve the subsurface-flow and solute-transport problems in cases with uncertain hydraulic permeability, Liao et al. [16] developed a nested sparse-grid-collocation method to quantify the uncertainty in numerical modeling of subsurface flow and solute transport. This novel method was much more efficient and robust than the traditional Monte-Carlo Method. In these numerical methods, the sizes of the grains and pores are conceptualized as a continuum according to the representative elementary volume. As indicated by Tran et al. [17], continuum-based methods may not accurately represent the heterogenous distributions of water pressure in the porous media associated with random arrangement of soil grains. Issues such as numerical oscillations near the wetting front, errors in maintaining mass balance and low computational efficiency can sometimes lead to large errors in the numerical solutions [11–13,18]. Moreover, these

methods are generally established on the assumption that water flow is averaged across the whole domain, including grains and pores, which contradicts the reality that underground water can flow only through the pore spaces in porous media.

Alternatively, the equivalent-pipe-network method was developed to model the sub-surface flow in porous media and fractured rock, such as the saturated flow in porous media [19], the unconfined seepage flow in fractured rock [20], the linear and nonlinear free-surface flow in porous media [21–23]. In the equivalent-pipe-network method, water flow is restricted to the sides of triangular elements and the hydraulic parameters of pipes are mathematically equivalent to the triangular elements. Thus, the numerical simulations are dependent on triangular mesh and the triangular elements around the free surface sometimes need to be updated iteratively [24]. Moreover, the equivalent-pipe-network models are established for isotropic media; they are not applicable to anisotropic media and are not interpreted physically.

Recently, Ye et al. [25,26] and Wei et al. [24] detailed a sound physical line-element model to solve the steady and transient free-surface flow in both isotropic and anisotropic media. Furthermore, Yuan et al. [27] extended this orthotropic line-element method to model the steady free-surface flow in three-dimensional porous media and a successful application on the left bank abutment slope of the Kajiwa Dam was achieved. Chen et al. [28] proposed a line-element approach on the unsteady free-surface flow in three-dimensional porous media with consideration of equivalent specific yield, and the effect of media anisotropy on the transient free-surface flow behavior was demonstrated. Due to the s of modeling free-surface flow in unconnected fracture networks, Ye et al. [29] developed a unified line-element method by reducing both the rock matrix and the fractures into one-dimensional line elements and included the effect of fracture distribution on the frees surface location. However, the flow velocity in the unsaturated area above the free surface is generally described by a continuous penalized Heaviside function, which is not consistent with the nonlinear results from Mualem [30] and Hu et al. [12]. Therefore, previous research works are limited in their ability to describe the saturated flow condition and do not account for the constitutive relationships between relative permeability, water content and pressure head. These models thus cannot be applied to rainfall seepage problems. Therefore, the line-element model is commonly used to describe unsaturated flow. The corresponding finite-line-element approach is also proposed as an extension of the saturated line-element model.

The primary objectives of this research are (1) to develop a simple line-element method with dimension reduction for modeling unsaturated flow in porous media and (2) to assess the numerical reliability of the proposed line-element method for different problems considering unsaturated flow. This research is organized as follows. In Section 2, the equivalent unsaturated hydraulic conductivity, flow velocity and continuity equations are derived. In Section 3, a dimension-reduced finite line-element method is proposed and combined with a complementary algorithm for Signorini's-type boundary conditions involving the seepage face boundary and infiltration boundary. In Section 4, the proposed model is validated by comparisons with the results from the available analytical, experimental and simulated approaches for unsaturated flow in a vertical soil column, unsaturated flow in a sand flume with drainage tunnels and transient unsaturated flow water-table recharge in a soil slab, respectively. The relationship of flow with mesh size and the time interval is also investigated.

2. Line-Element Model Development

2.1. Basic Equations

As shown in Figure 1, the two-dimensional unsaturated flow through the control volume based on the mass-balance principle is governed by Richards' equation [10]:

$$\frac{\partial \theta}{\partial t} = -\nabla \cdot v \tag{1}$$

where θ is the water content and v is the vector of flow velocity described by the Darcy-Buckingham law

$$v = -k_s k_r(\theta)\nabla(h+z) \tag{2}$$

where k_s is the tensor of saturated hydraulic conductivity, k_r is the relative hydraulic conductivity as a function of water content θ, h is the pressure head, and z is the vertical coordinate.
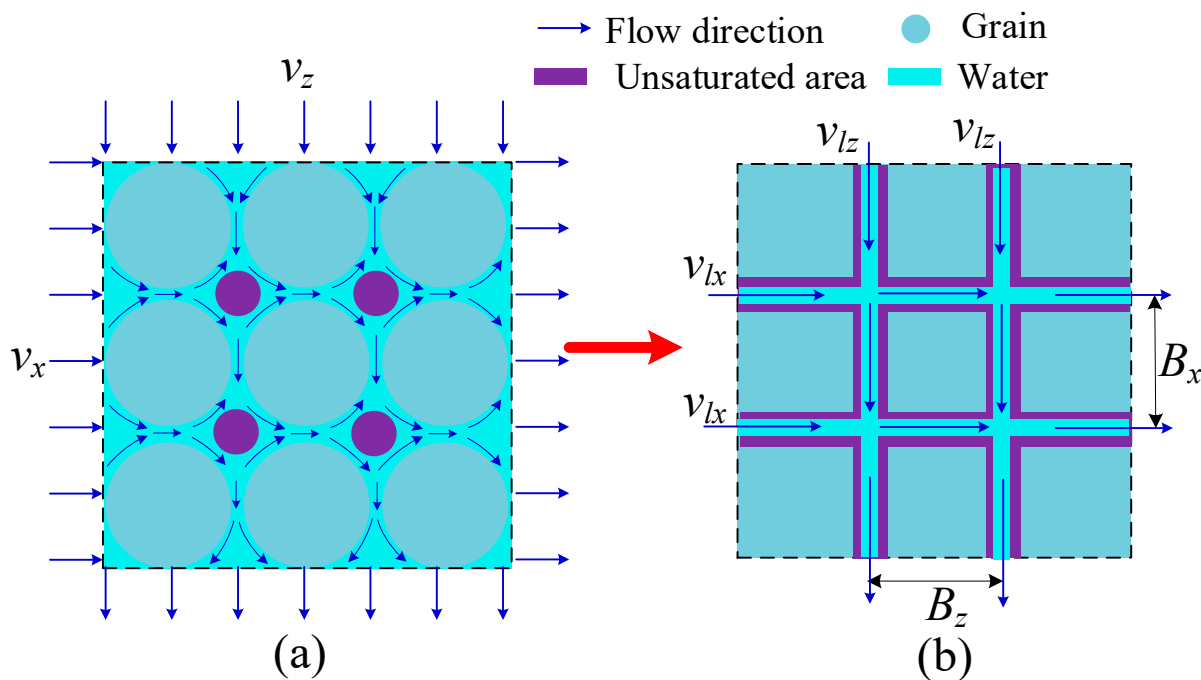

Figure 1. (**a**) The traditional continuum model; (**b**) The line-element model for unsaturated flow through the control volume (purple color denotes unsaturated void space).

2.2. Equivalent Flow Velocity and Relative Hydraulic Conductivity

As indicated by Ye et al. [25,26], the pores for flow conduction in the control volume can be substituted by an orthogonal network of horizontal and vertical channels. This model differs from the continuum hypothesis, which asserts that water flow should be averaged across the whole control volume. When the flow channels are commonly replaced by line elements, the equivalent hydraulic parameters and governing equations can also be derived based on the flux-equivalent principle. In an approach similar to the saturated-flow model, a homogeneous pore-scale pattern is employed to illustrate the behavior of unsaturated flow in the control volume, as presented in Figure 1a. The key difference is that only parts of the pore volume are occupied by water flow. Correspondingly, in the line-element model, the water flow is concentrated in the intermediate horizontal and vertical channels, as shown in Figure 1b. Therefore, water flow velocities in the unsaturated horizontal and vertical channels are also described by the Darcy-Buckingham law:

$$v_{lx} = k_{lx}\frac{\partial(h+z)}{\partial x} = k_{s,lx}k_{r,lx}(\theta_{lx})\frac{\partial(h+z)}{\partial x} \tag{3}$$

$$v_{lz} = k_{lz}\frac{\partial(h+z)}{\partial z} = k_{s,lz}k_{r,lz}(\theta_{lz})\frac{\partial(h+z)}{\partial z} \tag{4}$$

where the subscripts *lx* and *lz* are used to denote the horizontal and vertical channels, respectively, and v, k_s and k_r are the flow velocity, saturated and relative hydraulic conductivity of channels.

For the continuum model and the line-element model, the total rate Q_x on the inflow boundary in the horizontal direction, combining Equations (3) and (4), can be expressed as follows:

$$Q_x = v_x \cdot \Delta z = k_{s,x} k_r \frac{\partial (h+z)}{\partial x} \cdot \Delta z \tag{5}$$

$$Q_x = v_{lx} \cdot A_{lx} N_x = k_{s,lx} k_{r,lx} \frac{\partial (h+z)}{\partial x} \cdot A_{lx} N_x \tag{6}$$

where Δz is the vertical size of the control volume, N_x is the channel number in the vertical direction and A_{lx} is the area of single horizontal channel cross-section.

When water flows under saturated conditions such that $k_r = k_{r,lx} = 1$, Equations (5) and (6) are reduced to the saturated form, as stated by Ye et al. [20,21]. The saturated hydraulic conductivity of horizontal channels can thus be given as:

$$k_{s,lx} = k_{s,x} B_x / A_{lx} \tag{7}$$

where B_x is the horizontal channel spacing and is equal to $\Delta y / N_x$.

Inserting Equation (7) into Equation (6) and using $B_x = \Delta z / N_x$, we find

$$k_r = k_{r,lx} \tag{8}$$

Similarly, the saturated and relative hydraulic conductivities in the vertical direction between the continuum model and line-element model can be derived as

$$k_{s,lz} = k_{s,z} B_z / A_{lz} \tag{9}$$

$$k_r = k_{r,lz} \tag{10}$$

where A_{lz} and B_z are the cross-section area and channel spacing in the vertical direction. Equations (8) and (10) indicate that the equivalent relative hydraulic conductivity in the line-element model is equal to that in the continuum model.

Thus, Equations (3) and (4) can be rewritten as

$$v_{lx} = \frac{B_x}{A_{lx}} k_{s,x} k_r \frac{\partial (h+z)}{\partial x} \tag{11}$$

$$v_{lz} = \frac{B_z}{A_{lz}} k_{s,z} k_r \frac{\partial (h+z)}{\partial z} \tag{12}$$

Equations (11) and (12) indicate that the line-element model treats the flow around the channels as though it were flow into the channels.

2.3. Equivalent Continuity Equations

In the continuum model, the water content θ is averaged across the whole domain of the control volume. By contrast, in the line-element model, the water content θ is divided equally between the horizontal and vertical channels. The following equations can thus be obtained:

$$\theta_{lx} \cdot N_x A_{lx} \Delta x = \theta_{lz} \cdot N_z A_{lz} \Delta z = \frac{\theta}{2} \cdot \Delta x \Delta z \tag{13}$$

where θ_{lx} and θ_{lz} are the water content in the single horizontal and vertical channels.

Using $B_x = \Delta z / N_x$ and $B_z = \Delta x / N_z$ gives:

$$\theta_{lx} = \frac{\theta}{2} \frac{B_x}{A_{lx}} \tag{14}$$

$$\theta_{lz} = \frac{\theta}{2} \frac{B_z}{A_{lz}} \tag{15}$$

Based on mass-balance conservation, the total mass of inflow and outflow across the single horizontal channel is equal to the derivative of the water content over time. Thus, the continuity equation for the single horizontal channel can be given as

$$\frac{\partial \theta_{lx}}{\partial t} = \frac{\partial}{\partial x}\left[k_{s,lx}k_{r,lx}\frac{\partial(h+z)}{\partial x}\right] \tag{16}$$

Inserting Equations (11) and (14) into Equation (16) gives the equivalent continuity equation for the single horizontal channel:

$$\frac{1}{2}\frac{\partial \theta}{\partial t} = \frac{\partial}{\partial x}\left[k_{s,x}k_{r}\frac{\partial(h+z)}{\partial x}\right] \tag{17}$$

Similarly, the equivalent continuity equation for the single vertical channels is written as

$$\frac{1}{2}\frac{\partial \theta}{\partial t} = \frac{\partial}{\partial z}\left[k_{s,z}k_{r}\frac{\partial(h+z)}{\partial z}\right] \tag{18}$$

An interesting analogue of the continuity equation between the porous media and the orthotropic channels can be observed from Equations (1), (17) and (18): the final mathematical expressions are quite similar except that the coefficient in the water content term in the line-element model is half that in the continuum model, which is different from the equivalent one-to-one specific yield given by Chen et al. [28]. Note that only the vertical channels can contribute to water release/recharge during the unsteady saturated free-surface flow analysis, while the vertical and horizontal channels can contribute equally to the saturation variation in the control volume based on the average flow [10].

2.4. Unified Formulations and Boundary Condition

By comparing Equations (17) and (18) with Equation (1), the two-dimensional unsaturated flow problems through the porous media are reduced into one-dimensional form through an orthogonal network of line elements. Hence, a local coordinate *l.* as shown in Figure 2. is employed to replace the Cartesian coordinates *x* and *z*; the equivalent velocities in the Equations (11) and (12) can be generalized as:

$$v_{ij} = \frac{B_{ij}}{A_{ij}}k_{s}k_{r}\frac{\partial(h+z)}{\partial l} \tag{19}$$

where *i* and *j* denote the two endpoint numbers of an arbitrary horizontal or vertical line element.
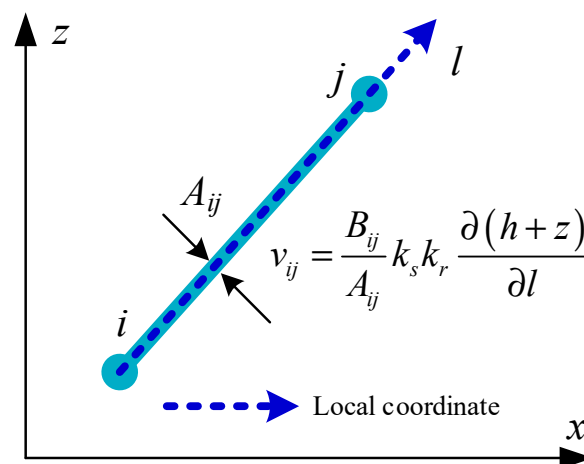

Figure 2. The local coordinate system of single fracture.

For simplicity, A_{ij} is assigned a unit of area, so Equation (19) is reduced to:

$$v_{ij} = B_{ij} k_s k_r \frac{\partial (h + z)}{\partial l} \tag{20}$$

The continuity Equations (17) and (18) can also be merged as

$$\frac{1}{2} \frac{\partial \theta}{\partial t} = \frac{\partial}{\partial l} \left[k_s k_r \frac{\partial (h + z)}{\partial l} \right] \tag{21}$$

Note that Equation (21) is similar to the h-based Richards' equation for one-dimensional unsaturated flow problems presented by Phoon et al. [18] and Berardi et al. [31], except for the 1/2 on the left side of Equation (21).

In order to solve the unsaturated flow problem based on the line-element model, Equation (21) should satisfy the following conditions:

(1)   Initial pressure-head condition

$$h_i|_{t=0} = h_0 \tag{22}$$

(2)   Dirichlet boundary condition

$$h_i(t) = \overline{h}_i(t) \tag{23}$$

(3)   Neumann boundary condition

$$q_i(t) = \overline{q}_i(t) \tag{24}$$

(4)   Signorini's-type boundary condition [12]

$$\begin{cases} h_i \leq h^*; q_i \leq q^* \\ (h_i - h^*)(q_i - q^*) = 0 \end{cases} \tag{25}$$

where h^* and q^* are the upper limits of pressure head and flux, respectively. The Signorini's-type boundary includes the seepage face boundary and the infiltration boundary. For the seepage boundary with $h^* = 0$ and $q^* = 0$, on the saturated part, $q_i \leq 0$, $h_i = 0$ while on the unsaturated part, $q_i = 0$, $h_i \leq 0$. For the infiltration boundary, on the saturated part, $q_i \leq q^*$, $h_i = h^*$ while on the unsaturated part, $q_i = q^*$, $h_i \leq h^*$.

3. Finite Line-Element Algorithm

When applying the variational principle and the specific moisture capacity $C = \partial \theta / \partial h$, the functional $I(h)$ of the continuity Equation (21) across the whole flow domain Ω yields

$$I(h) = \sum_\Omega \int_{l_{ij}} \frac{1}{2} k_s k_r \left[\frac{\partial (h + z)}{\partial l} \right]^2 dl + \sum_\Omega \int_{l_{ij}} \frac{C}{2} \frac{\partial h}{\partial t} h dl + \sum_\Gamma q_i h \tag{26}$$

where Γ is the Neumann boundary.

Minimizing the functional $I(h)$ gives

$$\frac{\partial I(h)}{\partial h_i} = \sum_\Omega \int_{l_{ij}} k_s k_r \frac{\partial (h + z)}{\partial l} \frac{\partial}{\partial h_i} \left[\frac{\partial (h + z)}{\partial l} \right] dl + \sum_\Omega \int_{l_{ij}} \frac{C}{2} \frac{\partial h}{\partial t} \frac{\partial h}{\partial h_i} dl + \sum_\Gamma q_i \frac{\partial h}{\partial h_i} = 0 \tag{27}$$

For the one-dimensional line element, the pressure head and coordinate can be expressed in the form of shape functions as follows:

$$h + z = N_i(h_i + z_i) + N_j(h_j + z_j) = \mathbf{N}(\mathbf{h}_e + \mathbf{z}_e) \tag{28}$$

$$N_i = 1 - l / l_{ij} \tag{29}$$

$$N_j = l/l_{ij} \tag{30}$$

$$\boldsymbol{N} = \begin{bmatrix} N_i & N_j \end{bmatrix} \tag{31}$$

$$\boldsymbol{h}_e = \begin{bmatrix} h_i & h_j \end{bmatrix}^{\mathrm{T}} \tag{32}$$

$$\boldsymbol{z}_e = \begin{bmatrix} z_i & z_j \end{bmatrix}^{\mathrm{T}} \tag{33}$$

where N_i and N_j are the one-dimensional shape functions in the local coordinate system and l_{ij} is the line length. The derivative of the shape functions N_i and N_j versus l can be obtained as:

$$\boldsymbol{B} = \begin{bmatrix} \frac{\partial N_i}{\partial l} & \frac{\partial N_j}{\partial l} \end{bmatrix} = \begin{bmatrix} -1/l_{ij} & 1/l_{ij} \end{bmatrix} \tag{34}$$

where $\boldsymbol{B}$ is the one-dimensional geometric matrix in the local coordinate system.

Then, the partial derivative terms in Equation (27) can be written as

$$\frac{\partial(h+z)}{\partial l} = -\frac{1}{l_{ij}}(h_i + z_i) + \frac{1}{l_{ij}}(h_j + z_j) = \boldsymbol{B}(\boldsymbol{h}_e + \boldsymbol{z}_e) \tag{35}$$

$$\left\{ \frac{\partial}{\partial h_i}\left[\frac{\partial(h+z)}{\partial l} \right] \quad \frac{\partial}{\partial h_j}\left[\frac{\partial(h+z)}{\partial l} \right] \right\} = \boldsymbol{B} \tag{36}$$

$$\begin{bmatrix} \frac{\partial h}{\partial h_i} & \frac{\partial h}{\partial h_j} \end{bmatrix} = \begin{bmatrix} N_i & N_j \end{bmatrix} = \boldsymbol{N} \tag{37}$$

Inserting Equations (35)–(37) into Equation (27) and using a back-difference method in the time domain, the finite-line-element matrix scheme for the unsaturated flow in porous media becomes

$$\left(\boldsymbol{K} + \frac{\boldsymbol{C}}{\Delta t} \right) \boldsymbol{h}^{\eta+1} = \frac{\boldsymbol{C}}{\Delta t} \boldsymbol{h}^{\eta} + \boldsymbol{R} \tag{38}$$

in which

$$\boldsymbol{K} = \sum_{\Omega} \int_{l_{ij}} \boldsymbol{B}^{\mathrm{T}} k_s k_r \boldsymbol{B} dl \tag{39}$$

$$\boldsymbol{C} = \sum_{\Omega} \int_{l_{ij}} \boldsymbol{N}^{\mathrm{T}} \frac{C}{2} \boldsymbol{N} dl \tag{40}$$

$$\boldsymbol{q} = \sum_{\Gamma} \boldsymbol{N}^{\mathrm{T}} \overline{q}_i - \sum_{\Omega} \int_{l_{ij}} \boldsymbol{B}^{\mathrm{T}} k_s k_r \boldsymbol{B} dl \cdot \boldsymbol{z} \tag{41}$$

where Δt is the time increment between time steps $\eta + 1$ and η. During the two successive iterations $m + 1$ and m, numerical solution is obtained when the following inequality is achieved:

$$\| \boldsymbol{h}_{m+1}^{\eta+1} - \boldsymbol{h}_m^{\eta+1} \| \le \delta \| \boldsymbol{h}_m^{\eta+1} \| \tag{42}$$

where δ is a preset tolerance with the value 0.001 in this study.

At each time step, it is not confirmed in advance whether the seepage face and infiltration boundaries are saturated or unsaturated. Therefore, a complementary algorithm for the Signorini's-type boundary conditions [12,32–34] is employed to determine saturated and unsaturated parts on the seepage face and infiltration boundaries. The algorithm at each time step is detailed as below:

(1) Initiate the iteration step at $m = 0$;
(2) Classify the nodes on the Signorini's-type boundary into two sets as $\mathbb{N}_1 = \{ i | h_i \le h^*; q_i = q^* \}$, $\mathbb{N}_2 = \{ i | h_i = h^*; q_i \le q^* \}$;
(3) For $i \in \mathbb{N}_1$ let $q_i = q^*$, while for $i \in \mathbb{N}_2$ let $h_i = h^*$. Solve Equation (38). If Equation (42) holds, end current calculation and turn to the next time step; else, turn to step (4);
(4) Update the node sets: if $i \in \mathbb{N}_1$ and $h_i > h^*$, then $\mathbb{N}_1 - \{ i \}$ and $\mathbb{N}_2 + \{ i \}$; if $i \in \mathbb{N}_2$ and $q_i > q^*$, then $\mathbb{N}_2 - \{ i \}$ and $\mathbb{N}_1 + \{ i \}$; turn to step (2).

4. Validations

4.1. One-Dimensional Infiltration in a Vertical Soil Column

The analytical solution for a one-dimensional infiltration through a vertical soil column, as developed by Warrick et al. [35], was first applied to verify the finite line-element method. This mathematical model contains one sandy clay loam layer 1 m in thickness, as shown in Figure 3. The relationships between the relative hydraulic conductivity, water content and pressure head are described by the van Genuchten-Mualem model [30,36]:

$$S_e = \frac{\theta - \theta_r}{\theta_s - \theta_r} = \begin{cases} (1 + |\alpha h|^n)^{-1+1/n} & h < 0 \\ 1 & h \geq 0 \end{cases} \tag{43}$$

$$k_r = S_e^{1/2}\left[1 - \left(1 - S_e^{1/m}\right)^m\right]^2 \tag{44}$$

where α and n are the constitutive parameters, S_e is the effective saturation and θ_s and θ_r are the saturated and residual water contents, respectively. Based on the curve-fitting experimental data from Phoon et al. [18], all the model parameters for the sandy clay loam soil were given as $k_s = 1 \times 10^{-6}$ m/s, $\theta_s = 0.363$, $\theta_r = 0.186$, $\alpha = 1$ m^{-1} and $n = 1.53$. The water pressure head through the whole flow domain was set at -8 m; that of the top boundary was set at 0 m.
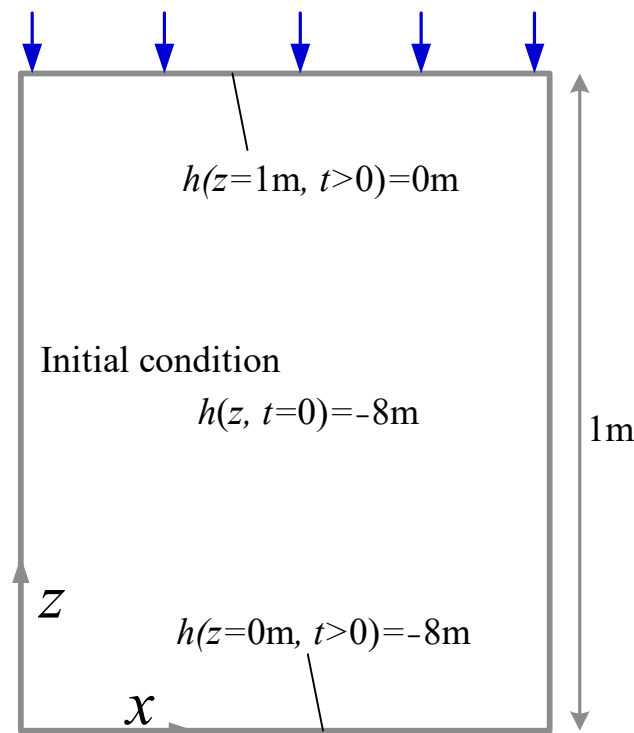

Figure 3. One-dimensional infiltration model from Warrick et al. [35].

To elucidate the mesh-size dependency of the line-element model, the soil column model was considered equivalent to three kinds of orthogonal networks of horizontal and vertical line elements with different spacings: $B_x = B_z = 0.01$ m, 0.02 m and 0.04 m, respectively. The time increment was fixed at 300 s for all three line-element models during analysis of unsaturated flow. Figure 4a shows the evolution over time of the pressure head along the depth based on the numerical simulations and analytical solutions from Warrick et al. [35]. The numerical curves from $B_x = B_z = 0.01$ m agree well with the analytical data, while the numerical predictions from $B_x = B_z = 0.02$ m and 0.04 m are generally higher than the theoretical results. Figure 4b shows the evolution of convergent iterative steps with

time, which indicates that the numerical solution can generally be obtained within 5 steps after 2 h.
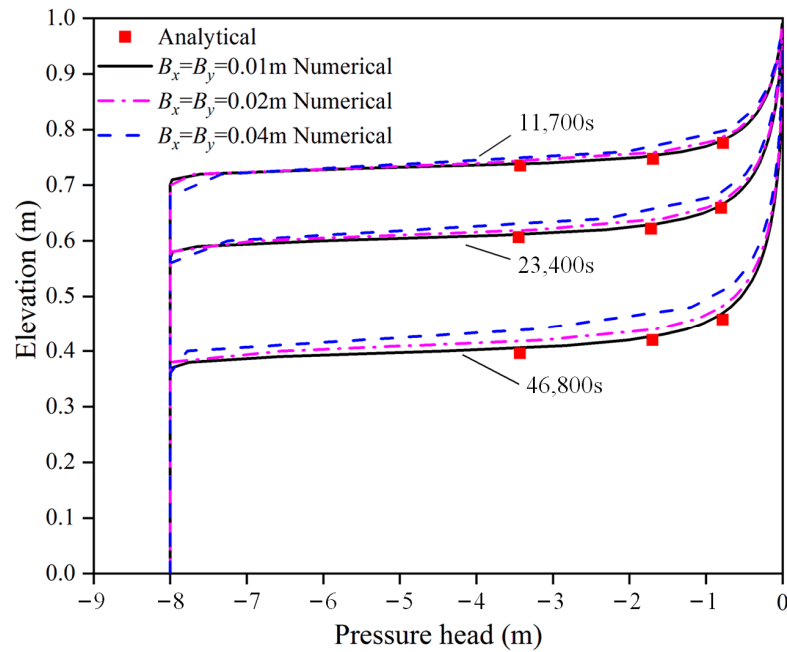
(**a**)
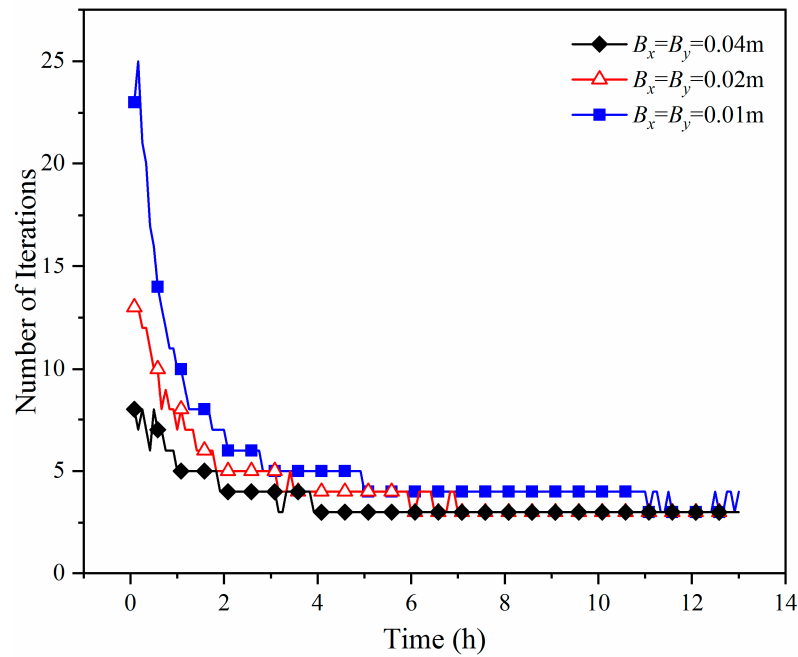
(**b**)

Figure 4. (**a**) The comparisons of analytical and numerical water pressure heads; (**b**) The evolution over time of convergent iterative steps with different spacings.

Figure 5a,b shows a plot of the evolution over time of water pressure heads along the depth and convergent iteration steps for four different time intervals from 100 s to 468 s, respectively. All mesh sizes were fixed as $B_x = B_z = 0.5$ m. Good agreements between the numerical results and analytical data were obtained for all time intervals. By comparison, there are almost no differences between the water-pressure curves from different time intervals. Nevertheless, the computational efficiencies from different time intervals vary, such as that the number of convergent iteration steps for $\Delta t = 100$ s is generally less than half

of that for Δt = 468 s. Thus, the fewer time intervals there are, the fewer convergent iteration steps are needed. Note that the number of convergent iteration steps decreases substantially in the beginning of the sampled time and then holds stable until the unsaturated flow gradually becomes steady.
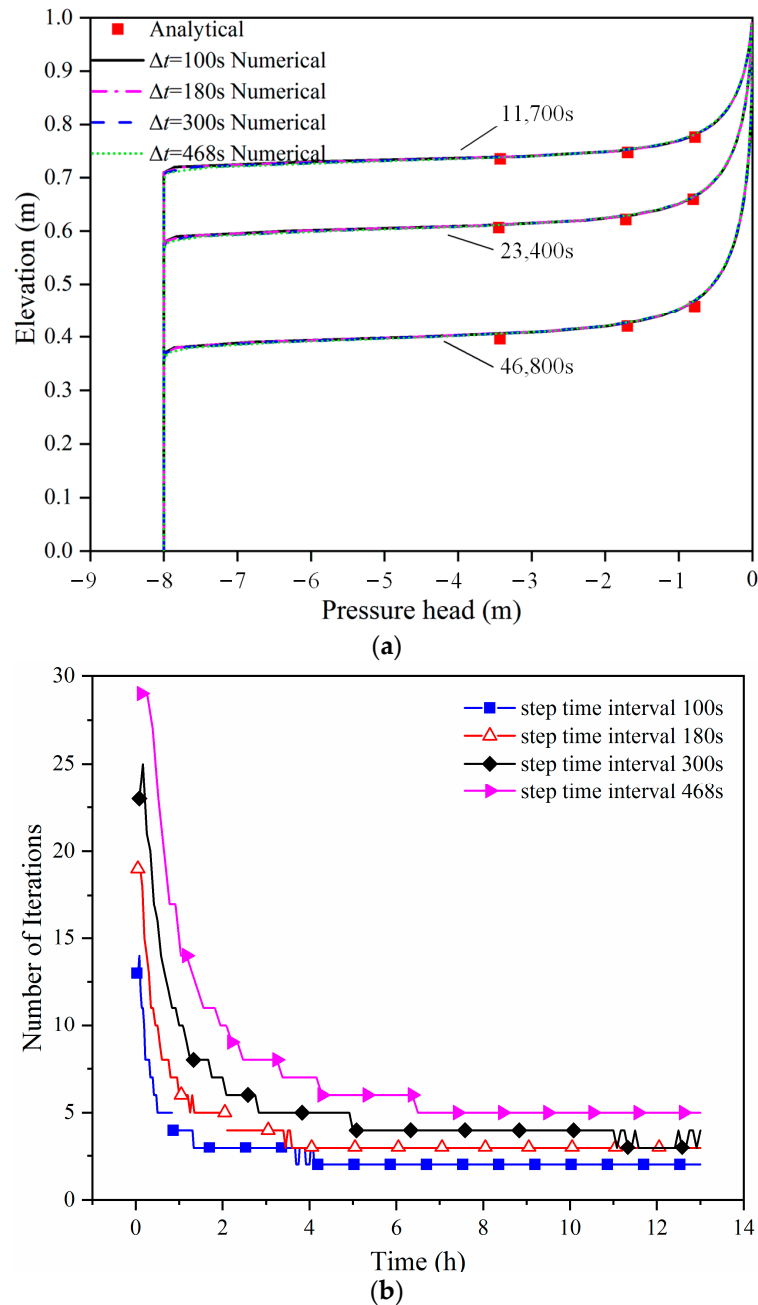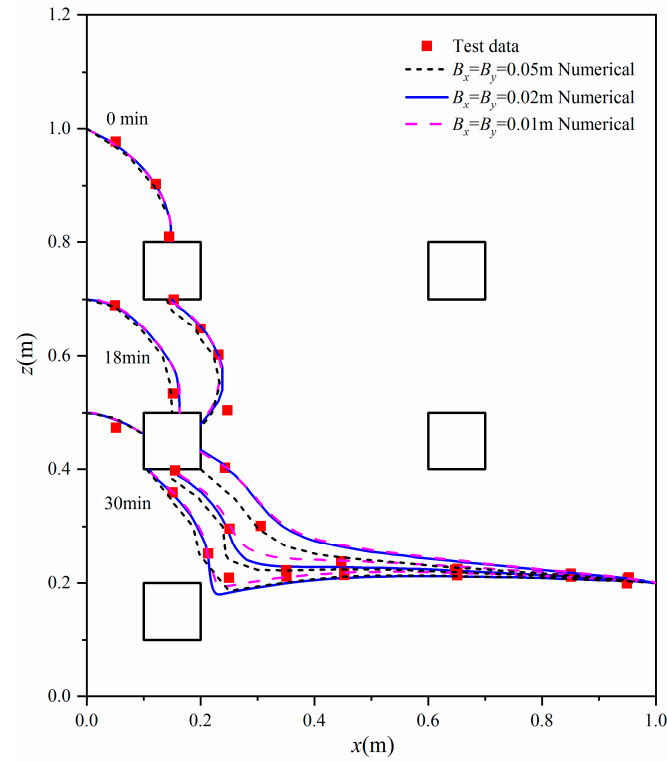

(a)

(b)

Figure 5. (**a**) The comparisons of analytical and numerical analyses of water pressure heads; (**b**) The evolution over time of convergent iterative steps with different time intervals.

4.2. Unsaturated Flow in a Sand Flume with Drainage Tunnels

The experimental observations of the unsaturated flow in a sand flume with drainage tunnels performed by Hu et al. [12] were used to validate the proposed numerical approach. The sand-flume model was created with a Perspex sheet and steel frame in the dimensions 1 m × 1.2 m. The upstream and downstream chambers were used to control water-level fluctuation using removable overflow plates. As shown in Figure 6, there were five drainage tunnels of dimensions 0.1 m × 0.1 m embedded in the sand flume. Based on the curve-fitting

experimental data from Hu et al. [12], all the van Genuchten-Mualem model parameters for the fine-sand soil were given as $k_s = 2.4 \times 10^{-5}$ m/s, $\theta_s = 0.363$, $\theta_r = 0$, $\alpha = 0.049$ m^{-1} and $n = 1.72$. During seepage, the initial upstream and downstream water levels were 1 m and 0.2 m, respectively; later, the upstream water level fell to 0.2 m with a constant speed of 1 m/s, while the downstream water level was invariable. The water head was measured using 34 piezometer tubes.

(a)
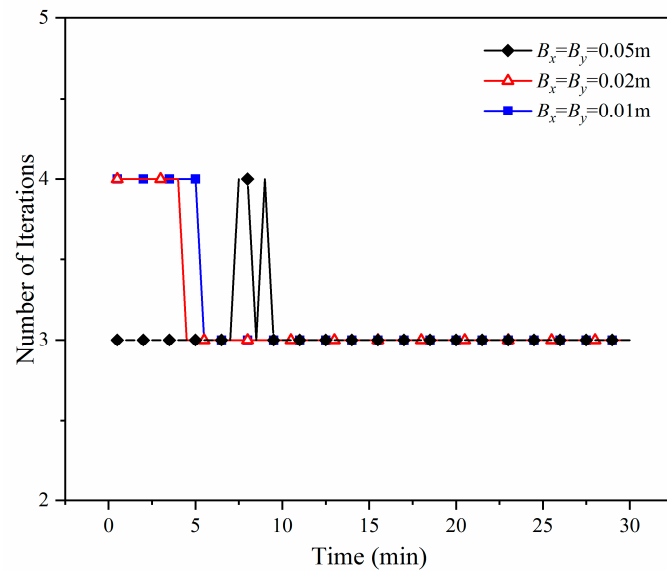
(b)

Figure 6. (**a**) The comparisons of analytical and numerical analyses of water pressure heads; (**b**) The evolution over time of convergent iterative steps with different spacings.

Similarly, the comparisons of water tables versus time between the numerical solutions and experimental observations for different mesh sizes and time intervals are shown in

Figures 6a and 7a, respectively. The numerical results generally are consistent with the experimental data, except that water tables from $B_x = B_z = 0.01$ m and 0.02 m at the initial time are higher in the numerical solutions than in the measurements. For a fine mesh $B_x = B_z = 0.01$ m, the comparisons of numerical calculations and test data indicate that the proposed line-element algorithm is weakly dependent on the time interval.
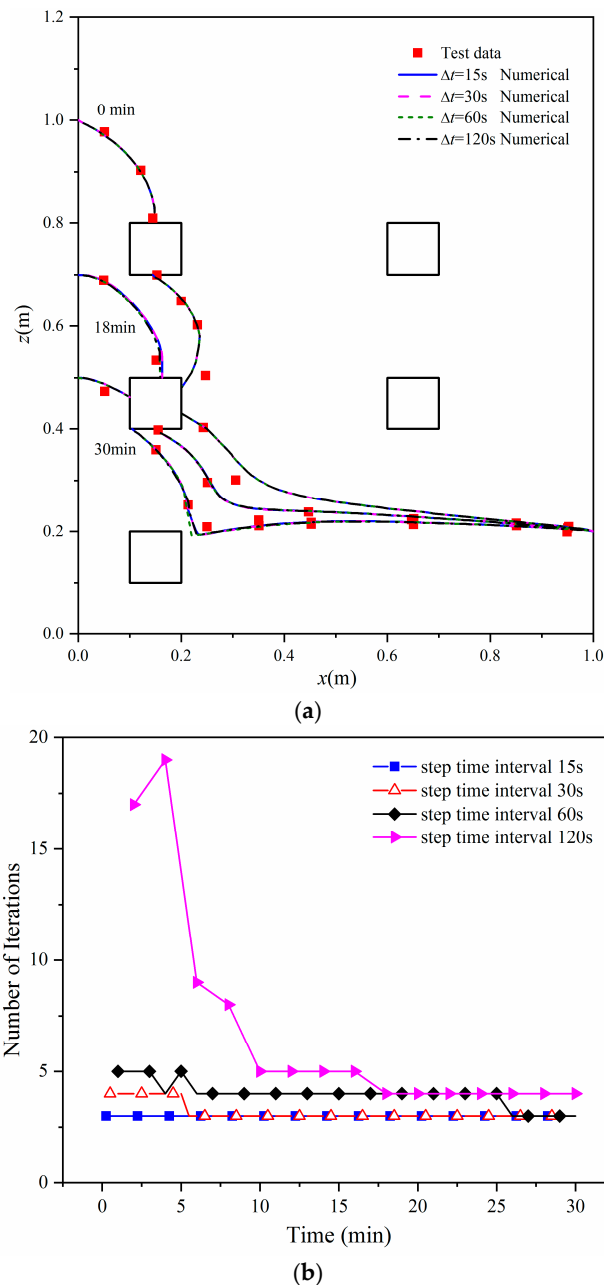

(a)

(b)

Figure 7. (**a**) The comparisons of analytical and numerical analyses of water pressure heads; (**b**) The evolution over time of convergent iterative steps with different time intervals.

Meanwhile, the corresponding convergent iteration steps are also presented in Figures 6b and 7b, respectively. For different mesh sizes, a maximum of four steps are required to reach convergence. For a fine mesh with $B_x = B_z = 0.01$ m, the time interval has negligible impact on the numerical accuracy but has a significant effect on the numerical convergence; the numerical solutions can be attained within five steps when the time interval is equal or less than 60 s.

4.3. Transient Unsaturated Flow Water-Table Recharge in a Soil Slab

　　The laboratory measurements of water pressure in a soil slab conducted by Vauclin et al. [37] were employed to assess the feasibility of applying the suggested finite line-element approach to infiltration problems. As shown in Figure 8, the model size was 3 m in length and 2 m in height. The left and bottom boundaries were impervious, and the right side was connected to a reservoir with a constant water level. The soil filling in the slab was a homogeneous fine river sand. Based on the curve-fitting experimental data from Vauclin et al. [37], the van Genuchten-Mualem model parameters for the fine river sand were given as k_s = 8.4 m/d, θ_s = 0.3, θ_r = 0.01, α = 3.3 m^{-1} and n = 4.1. During the infiltration process, the level of the water table was initially held constant at 0.65 m. Then, a constant flux of 0.148 m/h was supplied along the top left zone 0.5 m in width for 8 h. 20 tensiometers were evenly arranged in the soil slab to measure the water pressure head at different positions. The water table level was confirmed by visual observation of soil color.
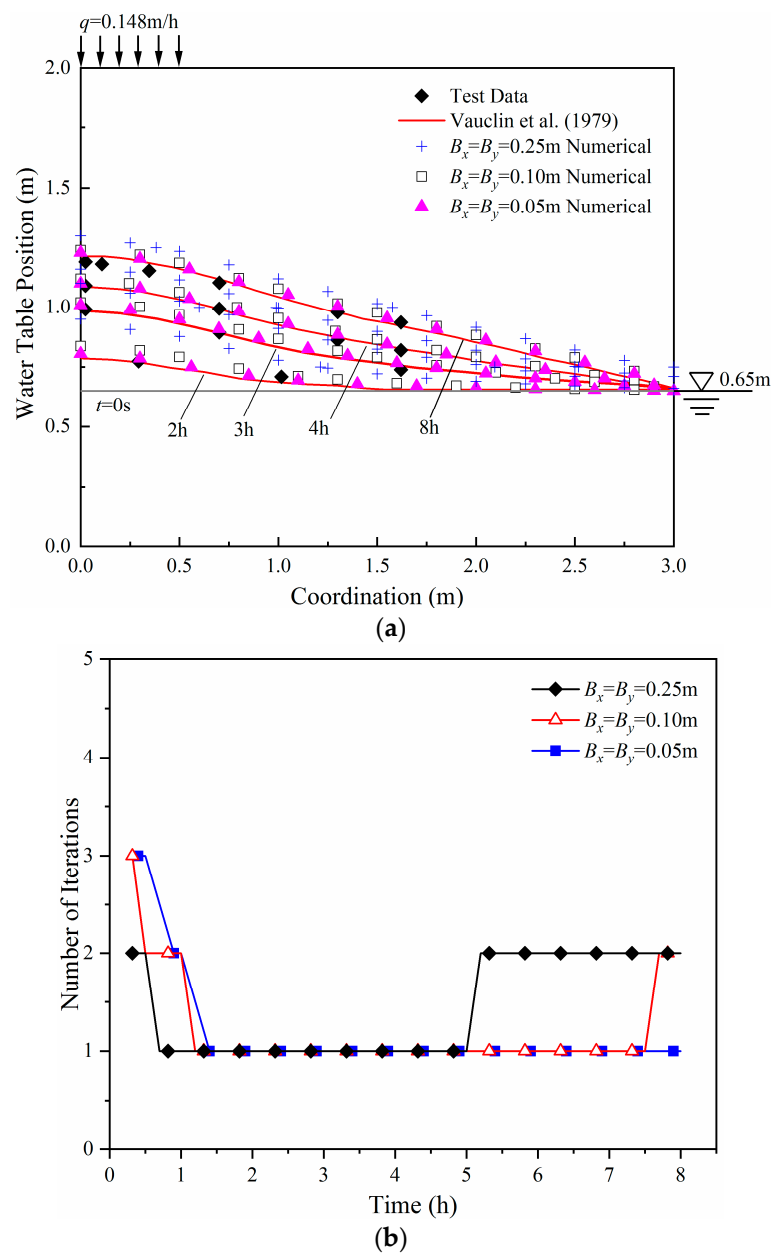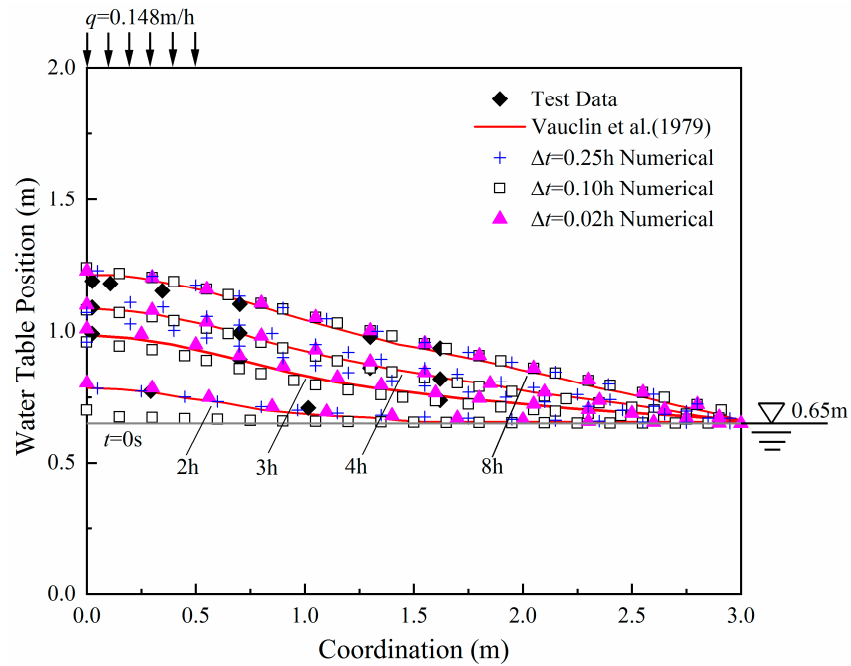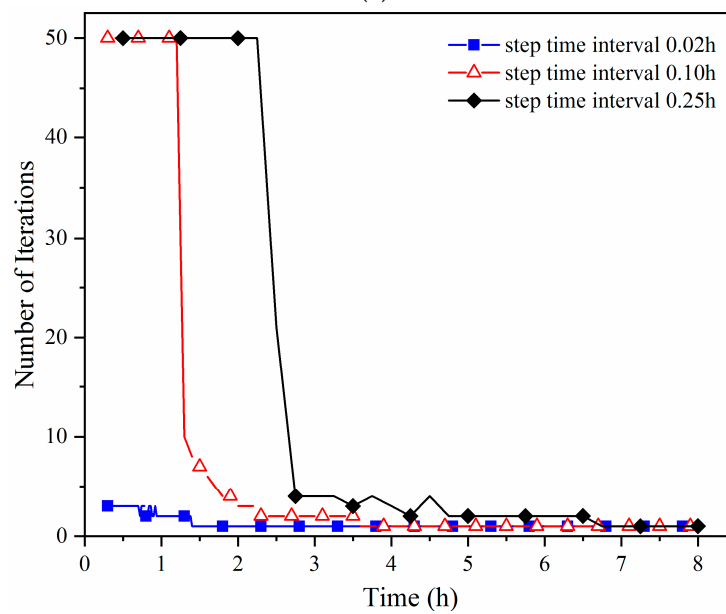

Figure 8. (**a**) The comparisons of analytical and numerical analyses of water pressure heads; (**b**) The evolution over time of convergent iterative steps with different spacings [37].

The simulated water tables varied with time, mesh size and interval size. The experimental results for different mesh sizes and time intervals are shown in Figures 8a and 9a, respectively. For different mesh sizes with $\Delta t = 0.02$ h, the numerical results from $B_x = B_z = 0.05$ m show good agreement with the experimental data, while the deviations from $B_x = B_z = 0.1$ m and 0.25 m yield results that are higher than the measurements. For a fine mesh $B_x = B_z = 0.01$ m, the numerical calculations from $\Delta t = 0.1$ h and 0.25 h are inconsistent with the experimental data, especially at time 2 h and 3 h. Additionally, the numerical predictions from an ADIPIT method [37] based on the continuum-based model are also given in Figures 8a and 9a; the proposed line-element method reproduces the unsaturated flow process of the continuum-based method with minimal deviation.

(**a**)

(**b**)

Figure 9. (**a**) The comparisons of analytical and numerical water pressure heads; (**b**) The evolution over time of convergent iterative steps with different time intervals [37].

The convergent iteration steps are presented in Figures 8b and 9b as well. The maximum step size to achieve convergence for different mesh sizes is 3. This result indicates the high convergence speed of the proposed line-element model. The computational efficiency of the model with $\Delta t = 0.02$ h is superior to that of the model with $\Delta t = 0.10$ h and that with $\Delta t = 0.25$ h. In contrast to the results seen from examples 1 and 2, the convergent iteration steps early in the process are very large when the time interval is equal to or greater than 0.10 h, the maximum iteration step size. The divergent numerical solutions early in the process when $\Delta t = 0.10$ h and 0.25 h, as shown in Figure 8a, may be the result of the sudden transition of some nodes from the unsaturated condition to the saturated condition with large time increments, which can cause significant changes in the specific moisture capacity and relative hydraulic conductivity, included in Equation (38), between two adjacent time steps.

5. Conclusions and Discussion

The traditional numerical methods were generally developed based on the continuum hypothesis, which states that the water flow is averaged over the whole domain, including both the pores and the grains. This assumption is contrary to the reality that underground water can flow only through the pore space in porous media. Thus, the line elements are used to characterize the flow channels and the equivalent flow velocity. Hydraulic parameters and governing equations are established in the line-element model on the basis of the flux-equivalent principle. In contrast to the traditional unsaturated flow model, there is no additional parameter in the line element. The relative hydraulic conductivity and specific moisture content are completely equivalent in these two models. The continuity equation is similar to that used in one-dimensional unsaturated flow problems in a vertical soil column, but the line-element model includes a coefficient of 1/2 in the water-content term.

The numerical line-element algorithm for unsaturated flow is proposed based on the variational principle, and the matrix forms are presented in one-dimensional form, such that the line integral is much more easily calculated in Equations (38)–(41). This ease of calculation is in contrast to the surface integral used in Equation (1). As a result, the nonlinearity of the unsaturated flow problem is highly reduced, and the numerical solution can be achieved rapidly, as demonstrated in the three illustrated example, regardless of mesh size or time interval. In fact, Equation (38) can be reduced to a one-dimensional line-element form for steady flow, as presented by Ye et al. [26], if the time interval approaches infinity. Compared with the line-element form for unsteady flow published by Ye et al. [25], Equation (38) transforms the free surface into a natural boundary; thus, the nonlinear iteration for free surface is no longer required. Additionally, the equivalent hydraulic radius and aperture are both eliminated from the calculation.

In order to assess the validity of the proposed finite line-element method in unsaturated flow with Signorini's-type boundary conditions, one-dimensional infiltration in a vertical soil column, unsaturated flow in a sand flume with drainage tunnels and transient unsaturated flow water-table recharge in a soil slab were employed. It was found that the numerical predictions from the proposed method show good agreement with the analytical, experimental and simulated results. In general, the proposed method is computationally efficient and sensitive to the mesh size and time interval. It is suggested that unsaturated flow be modeled with fine mesh and smaller time interval.

Herein, the line-element model has been successfully extended to model unsaturated flow in porous media, as well as steady and unsteady free-surface flow. The line-element model can thus be confidently used in many other scientific areas, such as heat transfer, solute transport and multiphase flow in porous media, given the similarity of governing equations. Note that the unsaturated flow is described by the Richards' equation and the Darcy-Buckingham law only for the water phase; the disturbance of other phases such as oil and gas was not investigated in this study. In order to describe multiphase flow in fractured porous media, a dynamic model with angular corners from Tørå et al. [38], a nested sparse grid-collocation method based on the three-phase black-oil model from Liao et al. [16],

and a two-phase flow unified-pipe-network method from Ren et al. [39] were developed. Considering the effects of capillary and viscous forces during immiscible two-phase fluid flow in porous media, crossover from capillary fingering to viscous fingering in a rough fracture [40] and faster finger flow in more ordered fracture networks [41,42] were observed. Further theoretical and numerical studies based on the line-element model are required to model multiphase flow behavior and its multifield coupling effect in future research.

Author Contributions: Conceptualization, M.L.; Methodology, X.Z., C.F., Q.Z. and L.Y.; Software, X.Z., C.F. and L.Y.; Validation, M.L., X.Z., C.F. and L.Y.; Investigation, M.L. and G.S.; Resources, M.L., G.S., Q.Z. and T.J.; Writing—original draft, X.Z., C.F. and L.Y.; Writing—review & editing, M.L., G.S., Q.Z. and T.J.; Funding acquisition, M.L., G.S., Q.Z. and T.J. All authors have read and agreed to the published version of the manuscript.

Data Availability Statement: Data are contained within the article.

Conflicts of Interest: Authors Min Li, Guoliang Su, Qiang Zhang and Tianyu Jing were employed by the company GD Power Inner Mongolia New Energy Development Co., Ltd. The remaining authors declare that the research was conducted in the absence of any commercial or financial relationships that could be construed as a potential conflict of interest.

References

1. Ghiassian, H.; Ghareh, S. Stability of sandy slopes under seepage conditions. *Landslides* **2008**, *5*, 397–406. [CrossRef]
2. Huang, F.; Chen, J.; Liu, W.; Huang, J.; Hong, H.; Chen, W. Regional rainfall-induced landslide hazard warning based on landslide susceptibility mapping and a critical rainfall threshold. *Geomorphology* **2022**, *408*, 108236. [CrossRef]
3. Zhu, S.R.; Wu, L.Z.; Huang, J. Application of an improved P (m)-SOR iteration method for flow in partially saturated soils. *Comput. Geosci.* **2022**, *26*, 131–145. [CrossRef]
4. Yao, C.; Wu, L.; Yang, J.; Xiao, L.; Liu, X.; Jiang, Q.; Zhou, C. Influences of tailings particle size on overtopping tailings dam failures. *Mine Water Environ.* **2021**, *40*, 174–188. [CrossRef]
5. Ye, Z.; Yang, J. Experimental study of real-time temperature-dependent nonlinear deformation of sandstone. *Fuel* **2023**, *354*, 9062569. [CrossRef]
6. Chen, Y.-F.; Ye, Y.; Hu, R.; Yang, Z.; Zhou, C.-B. Modeling unsaturated flow in fractured rocks with scaling relationships between hydraulic parameters. *J. Rock Mech. Geotech. Eng.* **2022**, *14*, 1697–1709. [CrossRef]
7. Kacimov, A.R.; Yakimov, N.D.; Šimůnek, J. Phreatic seepage flow through an earth dam with an impeding strip. *Comput. Geosci.* **2019**, *24*, 17–35. [CrossRef]
8. Ma, Y.; Meng, X.; Yao, C.; Zhang, X.; Dong, W.; Jiang, Q.; Li, Y.; Zhou, C. Electro-mechanical impedance technique for concrete strength monitoring: Three-dimensional model development and experimental verification. *Measurement* **2023**, *222*, 113558. [CrossRef]
9. Sun, H.; Xiong, F.; Wu, Z.; Ji, J.; Fan, L. An extended numerical manifold method for two-phase seepage–stress coupling process modelling in fractured porous medium. *Comput. Methods Appl. Mech. Eng.* **2022**, *391*, 114514. [CrossRef]
10. Richards, L.A. Capillary conduction of liquids through porous mediums. *Physics* **1931**, *1*, 318–333. [CrossRef]
11. Wu, M. A finite-element algorithm for modeling variably saturated flows. *J. Hydrol.* **2010**, *394*, 315–323. [CrossRef]
12. Hu, R.; Chen, Y.F.; Zhou, C.B.; Liu, H.H. A numerical formulation with unified unilateral boundary condition for unsaturated flow problems in porous media. *Acta Geotech.* **2017**, *12*, 277–291. [CrossRef]
13. Celia, M.; Efthimios, A.; Bouloutas, T.; Rebecca, L. A general mass-conservative numerical solution for the unsaturated flow equation. *Water Resour. Res.* **1990**, *26*, 1483–1496. [CrossRef]
14. Eymard, R.; Gutnic, M.; Hilhorst, D. The finite volume method for Richards equation. *Comput. Geosci.* **1999**, *3*, 259–294. [CrossRef]
15. Zheng, H.; Liu, F.; Li, C. Primal mixed solution to unconfined seepage flow in porous media with numerical manifold method. *Appl. Math. Model.* **2015**, *39*, 794–808. [CrossRef]
16. Liao, Q.; Zhang, D.; Tchelepi, H. Nested sparse grid collocation method with delay and transformation for subsurface flow and transport problems. *Adv. Water Resour.* **2017**, *104*, 158–173. [CrossRef]
17. Tran, K.M.; Bui, H.H.; Nguyen, G.D. DEM modelling of unsaturated seepage flows through porous media. *Comput. Part. Mech.* **2022**, *9*, 135–152. [CrossRef]
18. Phoon, K.K.; Tan, T.S.; Chong, P.C. Numerical simulation of Richards equation in partially saturated porous media: Under-relaxation and mass balance. *Geotech. Geol. Eng.* **2007**, *25*, 525–541. [CrossRef]
19. Xu, Z.; Ma, G.; Li, S. A Graph-theoretic Pipe Network Method for water flow simulation in a porous medium: GPNM. *Int. J. Heat Fluid Flow* **2014**, *45*, 81–97. [CrossRef]

20. Ren, F.; Ma, G.; Wang, Y.; Fan, L. Pipe network model for unconfined seepage analysis in fractured rock masses. *Int. J. Rock Mech. Min. Sci.* **2016**, *88*, 183–196. [CrossRef]
21. Abareshi, M.; Hosseini, S.M.; Sani, A.A. Equivalent pipe network model for a coarse porous media and its application to 2d analysis of flow through rockfill structures. *J. Porous Media* **2017**, *20*, 303–324. [CrossRef]
22. Afzali, S.H.; Monadjemi, P. Simulation of flow in porous media: An experimental and modeling study. *J. Porous Media* **2014**, *17*, 469–481. [CrossRef]
23. Moosavian, N. Pipe network modeling for analysis of flow in porous media. *Can. J. Civ. Eng.* **2019**, *46*, 1151–1159. [CrossRef]
24. Wei, W.; Jiang, Q.; Ye, Z.; Xiong, F.; Qin, H. Equivalent fracture network model for steady seepage problems with free surfaces. *J. Hydrol.* **2021**, *603*, 127156. [CrossRef]
25. Ye, Z.; Fan, Q.; Huang, S.; Cheng, A. A one-dimensional line element model for transient free surface flow in porous media. *Appl. Math. Comput.* **2021**, *392*, 125747. [CrossRef]
26. Ye, Z.; Qin, H.; Chen, Y.; Fan, Q. An equivalent pipe network model for free surface flow in porous media. *Appl. Math. Model.* **2020**, *87*, 389–403. [CrossRef]
27. Yuan, Q.; Yin, D.; Chen, Y. A Simple Line-Element Model for Three-Dimensional Analysis of Steady Free Surface Flow through Porous Media. *Water* **2023**, *15*, 1030. [CrossRef]
28. Chen, Y.; Yuan, Q.; Ye, Z.; Peng, Z. A Dimension-Reduced Line Element Method for 3D Transient Free Surface Flow in Porous Media. *Water* **2023**, *15*, 3072. [CrossRef]
29. Ye, Z.; Xiong, Y.; Xiong, F.; Zhang, Q. An equivalent line element approach for free surface flow through two-dimensional rock mass including fracture networks. *Appl. Math. Comput.* **2023**, *453*, 129308. [CrossRef]
30. Mualem, Y. A new model for predicting the hydraulic conductivity of unsaturated porous media. *Water Resour. Res.* **1976**, *12*, 513–522. [CrossRef]
31. Berardi, M.; Difonzo, F.; Vurro, M.; Lopez, L. The 1D Richards' equation in two layered soils: A Filippov approach to treat discontinuities. *Adv. Water Resour.* **2018**, *115*, 264–272. [CrossRef]
32. Chen, Y.; Hu, R.; Zhou, C.; Li, D.; Rong, G. A new parabolic variational inequality formulation of Signorini's condition for non-steady seepage problems with complex seepage control systems. *Int. J. Numer. Anal. Methods Geomech.* **2011**, *35*, 1034–1058. [CrossRef]
33. Zheng, H.; Liu, D.F.; Lee, C.F.; Tham, L.G. A new formulation of Signorini's type for seepage problems with free surfaces. *Int. J. Numer. Methods Eng.* **2005**, *64*, 1–16. [CrossRef]
34. Ye, Z.; Jiang, Q.; Zhou, C.; Liu, Y. Numerical analysis of unsaturated seepage flow in two-dimensional fracture networks. *Int. J. Geomech.* **2017**, *17*, 04016118. [CrossRef]
35. Warrick, A.W.; Lomen, D.O.; Yates, S.R. A generalized solution to infiltration. *Soil Sci. Soc. Am. J.* **1985**, *49*, 34–38. [CrossRef]
36. van Genuchten, M.T. A closed-form equation for predicting the hydraulic conductivity of unsaturated soils. *Soil Sci. Soc. Am. J.* **1980**, *44*, 892–898. [CrossRef]
37. Vauclin, M.; Khanji, D.; Vauchaud, G. Experimental and numerical study of a transient two-dimensional unsaturated–saturated water table problem. *Water Resour. Res.* **1979**, *15*, 1089–1101. [CrossRef]
38. Tørå, G.; Øren, P.-E.; Hansen, A. A dynamic network model for two-phase flow in porous media. *Transp. Porous Media* **2011**, *92*, 145–164. [CrossRef]
39. Ren, F.; Ma, G.; Wang, Y.; Fan, L.; Zhu, H. Two-phase flow pipe network method for simulation of CO2 sequestration in fractured saline aquifers. *Int. J. Rock Mech. Min. Sci.* **2017**, *98*, 39–53. [CrossRef]
40. Chen, Y.F.; Fang, S.; Wu, D.S.; Hu, R. Visualizing and quantifying the crossover from capillary fingering to viscous fingering in a rough fracture. *Water Resour. Res.* **2017**, *53*, 7756–7772. [CrossRef]
41. Ye, Z.; Fan, X.; Zhang, J.; Sheng, J.; Chen, Y.; Fan, Q.; Qin, H. Evaluation of connectivity characteristics on the permeability of two-dimensional fracture networks using geological entropy. *Water Resour. Res.* **2021**, *57*, 128081. [CrossRef]
42. Ye, Z.; Jiang, Q.; Yao, C.; Liu, Y.; Cheng, A.; Huang, S.; Liu, Y. The parabolic variational inequalities for variably saturated water flow in heterogeneous fracture networks. *Geofluids* **2018**, *2018*, 1–16. [CrossRef]